Simple lattice Boltzmann subgrid-scale model for convectional flows with high Rayleigh numbers within an enclosed circular annular cavity

Sheng Chen,[1,2] Jonas Tölke,[2] and Manfred Krafczyk[2,*]
[1]*State Key Laboratory of Coal Combustion, Huazhong University of Science and Technology, Wuhan 430074, China*
[2]*Institute for Computational Modeling in Civil Engineering, Technical University, Braunschweig 38106, Germany*
(Received 20 March 2009; published 11 August 2009)

Natural convection within an enclosed circular annular cavity formed by two concentric vertical cylinders is of fundamental interest and practical importance. Generally, the assumption of axisymmetric thermal flow is adopted for simulating such natural convections and the validity of the assumption of axisymmetric thermal flow is still held even for some turbulent convection. Usually the Rayleigh numbers (Ra) of realistic flows are very high. However, the work to design suitable and efficient lattice Boltzmann (LB) models on such flows is quite rare. To bridge the gap, in this paper a simple LB subgrid-scale (SGS) model, which is based on our recent work [S. Chen, J. Tölke, and M. Krafczyk, Phys. Rev. E **79**, 016704 (2009); S. Chen, J. Tölke, S. Geller, and M. Krafczyk, Phys. Rev. E **78**, 046703 (2008)], is proposed for simulating convectional flow with high Ra within an enclosed circular annular cavity. The key parameter for the SGS model can be quite easily and efficiently evaluated by the present model. The numerical experiments demonstrate that the present model works well for a large range of Ra and Prandtl number (Pr). Though in the present study a popularly used static Smagorinsky turbulence model is adopted to demonstrate how to develop a LB SGS model for simulating axisymmetric thermal flows with high Ra, other state-of-the-art turbulence models can be incorporated into the present model in the same way. In addition, the present model can be extended straightforwardly to simulate other axisymmetric convectional flows with high Ra, for example, turbulent convection with internal volumetric heat generation in a vertical cylinder, which is an important simplified representation of a nuclear reactor.

DOI: 10.1103/PhysRevE.80.026702 PACS number(s): 47.11.−j

I. INTRODUCTION

An enclosed circular annular cavity formed by two concentric vertical cylinders, containing a fluid through which heat is transferred by natural convection, is a simplified representation of a number of practical applications [1–4]. For example, a commonly used apparatus for the measurement of the thermal conductivity of a fluid consists of an electrically heated wire mounted on the axis of a cylinder containing the fluid. Here, the ratio of the outer and inner radii of the annulus is large. Another example is provided by the annular space which is sometimes formed between the core of a nuclear reactor and the surrounding shield or pressure vessel. This space may be closed at each end and filled with a gas to provide thermal insulation. In this situation the radius ratio is not much bigger than unity. The limiting case of radius ratio equal to unity represents a cavity formed by two plane walls [5–8]. A considerable amount of both analytical and experimental works has been devoted to this problem [1,2,9]. Generally, the approximation of axisymmetric thermal flow is adopted for simulating such natural convections [9–11]. With cylinder coordinates, only one half of the whole domain needs to be computed, so the computational cost is significantly reduced [4,11,12]. And for some convectional flows with high Rayleigh numbers, even for some turbulent convection, this approximation of axisymmetric thermal flow is still adopted [11–14]. Of course the realistic turbulence is always three dimensions, but it is usually too expensive for available computer capability to simulate, especially for practical industrial applications. This two-dimensional approximation is proposed due to the balance between numerical accuracy and computational efficiency and numerous works have validated it by experimental investigation as well as numerical simulation [11–24]. For example, in Refs. [17,18] Berg and co-workers made comparisons between the results obtained by three-dimensional simulation and that obtained by this two-dimensional approximation for turbulent flow during alloying process and claimed that the analysis can be conducted in two dimensions with only small losses of accuracy. Poole and Escudier [20] showed that there realistically existed axisymmetric turbulent flow within an axisymmetric domain, both for non-Newtonian fluid and for Newtonian fluid, by experiments. In Refs. [12,16] Sharma *et al.* and Xu *et al.* demonstrated that the numerical results obtained by this two-dimensional approximation agreed well with the experimental data for turbulent flows. Consequently to date this two-dimensional approximation is popularly used varying from steel and nuclear industries to fundamental investigation, especially for turbulent natural convection within axisymmetric space [11–13], which is simulated in the present study. Some turbulence models, for example, $k-\epsilon$ and subgrid-scale (SGS) models, are introduced for simulating such axisymmetric thermal flows with high Rayleigh numbers [11–14]. In addition, this axisymmetric approximation and the evolution of vorticity density field also play important roles in the statistical equilibrium theory for turbulence research. For readers interesting in this field please see a recent publication [25] and references therein.

Although the lattice Boltzmann (LB) method has matured for simulating and modeling complicated physical, chemical, and social systems [26–42], the attempts to employ the LB

*kraft@irmb.tu-bs.de

models to simulate the axisymmetric thermal flows mentioned above are quite sparse. The main difficulty results from the intrinsic shortcoming of the standard LB models [43–45]: the standard LB models are based on the Cartesian coordinate system, therefore we have to use a three-dimensional LB model to solve such quasi-two-dimensional axisymmetric problems, in which the cubic lattices and a treatment of curved boundary are used. This implies that one or more dimensional lattices are required for simulation of the flows and hence the computational efficiency is significantly reduced. In order to overcome the difficulty to improve computational efficiency, Peng *et al.* [46] designed a cylinder-coordinate-based hybrid LB scheme to simulate axisymmetric thermal flows. In their model, the axial and radial velocity components are solved by the Halliday-type axisymmetric LB model [47]; the azimuthal velocity and the temperature are solved by the central difference scheme. However, because hampered by the numerical instability of the hybrid scheme, their discussion was limited in a very narrow range with low Rayleigh numbers. It was found that, even with very fine grid resolutions, the hybrid LB scheme proposed by Peng *et al.* is still unstable for simulating axisymmetric thermal flows with high Rayleigh number [48]. Later, Huang *et al.* [48] proposed an improved version of the model of Peng *et al.* for axisymmetric thermal flows. In the model of Huang *et al.*, an incompressible lattice two-dimensional nine-speed (D2Q9) model is used instead of the standard lattice D2Q9 model in the scheme of Peng *et al.* to improve the numerical stability. Although the hybrid LB scheme of Huang *et al.* is more numerically stable than that of Peng *et al.*, due to the intrinsic disadvantages of the Halliday-type LB model, too many complicated force terms existing in the model of Huang *et al.* and a great deal of lattice grids are still required to guarantee numerical stability [43,44,48], which means the huge demand of computational resources and makes the improved hybrid LB scheme too expensive to simulate practical cases. Moreover, if there exists additional internal or external forcing, the calculating process of these models will become more complicated because the fluid velocity and the equilibrium velocity both have to be redefined [43]. Recently, the present authors proposed a simple cylinder-coordinate-based LB model for axisymmetric thermal flows [49], which is based on our previous work to solve vorticity-stream-function equations by the LB method [30,43]. In this simple model the flow field and the temperature field both are solved by the two-dimensional five-speed (D2Q5) lattice model, and almost all defects in previous models for simulating axisymmetric thermal flows are overcame.

However, the attempt to design a cylinder-coordinate-based LB model for axisymmetric thermal flows with high Rayleigh numbers is absent yet, which hampers using the LB method for practical simulations. In order to bridge this gap, in this paper, we design a simple lattice Boltzmann SGS model, which is based on our previous work [43,49], to simulate axisymmetric thermal flows with high Rayleigh numbers. The present model is based on the large-eddy simulation (LES) technique. What should be mentioned is that although in the present study a popularly used static Smagorinsky turbulence model is adopted to demonstrate how to develop a LB SGS model for simulating axisymmetric thermal flows with high Rayleigh numbers, other state-of-the-art turbulence models [50–52] can be incorporated into the present model in the same way.

The spirit of LES-based LB models is to split the effective fluid viscosity ν_e into two parts, ν_0 and ν_t [53–57]. ν_0 is the molecular viscosity and ν_t is the eddy viscosity. Although the LES has been popularly used in the existing LB models [53–59], the present work is still quite original because previous work just discussed how to incorporate turbulence models into the primitive-variable-based LB models, which is helpless for the present study due to the present model basing on vorticity-stream-function equations. In addition, generally in the primitive-variable LES-based LB models the calculation of the effective lattice relaxation time (τ_e), which depends on ν_e, is complicated either in the Bhatnagar-Gross-Krook approximation [53,54,58] or in multiple-relaxation-time models [55,56], and for some cases to obtain the exact value of τ_e is extremely difficult [57,60]. However, in Sec. III, we will show that the calculation of τ_e in the present model is much simpler and more efficient than that in primitive-variable LES-based LB models due to the intrinsic features of the present model.

The rest of the paper is organized as follows. the LES-based governing equations for axisymmetric thermal flows is presented in Sec. II. In Sec. III, a simple cylinder-coordinate-based axisymmetric thermal LB SGS model is introduced. In Sec. IV, numerical experiments are performed to validate the present model. Summary and conclusion are presented in Sec. V.

II. LES-BASED GOVERNING EQUATIONS FOR AXISYMMETRIC THERMAL FLOWS

With the Boussinesq assumption, the LES-based primitive-variable-based governing equations for axisymmetric thermal flows in the cylindrical coordinate system can be written as [12–14,57,60–63]

$$\frac{\partial u}{\partial r} + \frac{u}{r} + \frac{\partial w}{\partial z} = 0, \tag{1}$$

$$\frac{\partial u}{\partial t} + u\frac{\partial u}{\partial r} + w\frac{\partial u}{\partial z} = -\frac{1}{\rho}\frac{\partial p}{\partial r} + \nu_e \nabla^2 u, \tag{2}$$

$$\frac{\partial w}{\partial t} + u\frac{\partial w}{\partial r} + w\frac{\partial w}{\partial z} = -\frac{1}{\rho}\frac{\partial p}{\partial z} + \nu_e \nabla^2 w + g\alpha\Delta T, \tag{3}$$

$$\frac{\partial T}{\partial t} + u\frac{\partial T}{\partial r} + w\frac{\partial T}{\partial z} = D_e \nabla^2 T, \tag{4}$$

where

$$\nabla^2 = \frac{1}{r}\frac{\partial}{\partial r}\left(r\frac{\partial}{\partial r}\right) + \frac{\partial^2}{\partial z^2}.$$

u and w are radial and axial velocity components, p is the pressure, T is the temperature, ν_e is the effective kinetic viscosity, g is the gravitational acceleration along the negative z

axis, D_e is the effective thermal conductivity, ρ is the density, ΔT is the temperature difference, and α is the coefficient of thermal expansion.

For axisymmetric flow, computation time can be reduced if the problem is reformulated so that the three variables u, w, and p are eliminated in favor of the vorticity ω and Stokes stream function ψ [14,43,49], which are defined as

$$\omega = \frac{\partial w}{\partial r} - \frac{\partial u}{\partial z}, \tag{5}$$

$$u = \frac{1}{r}\frac{\partial \psi}{\partial z}, \tag{6}$$

$$w = -\frac{1}{r}\frac{\partial \psi}{\partial r}. \tag{7}$$

The dimensionless vorticity-stream-function-based governing equations read [12–14,57,62]

$$\frac{\partial \tilde{S}}{\partial \tilde{t}} + \tilde{u}\frac{\partial \tilde{S}}{\partial \tilde{r}} + \tilde{w}\frac{\partial \tilde{S}}{\partial \tilde{z}} = \mathrm{Pr}\frac{1}{\tilde{r}}\frac{\partial \tilde{T}}{\partial \tilde{r}} + \tilde{\nu}_e\left\{\frac{1}{\tilde{r}}\frac{\partial}{\partial \tilde{r}}\left[\frac{1}{\tilde{r}}\frac{\partial}{\partial \tilde{r}}(\tilde{r}^2\tilde{S})\right] + \frac{\partial^2 \tilde{S}}{\partial \tilde{z}^2}\right\}, \tag{8}$$

$$\frac{\partial \tilde{T}}{\partial \tilde{t}} + \tilde{u}\frac{\partial \tilde{T}}{\partial \tilde{r}} + w\frac{\partial \tilde{T}}{\partial \tilde{z}} = \tilde{D}_e\left[\frac{1}{\tilde{r}}\frac{\partial}{\partial \tilde{r}}\left(\tilde{r}\frac{\partial \tilde{T}}{\partial \tilde{r}}\right) + \frac{\partial^2 \tilde{T}}{\partial \tilde{z}^2}\right], \tag{9}$$

$$\frac{\partial}{\partial \tilde{r}}\left(\frac{1}{\tilde{r}}\frac{\partial \tilde{\psi}}{\partial \tilde{r}}\right) + \frac{1}{\tilde{r}}\frac{\partial^2 \tilde{\psi}}{\partial \tilde{z}^2} = -\tilde{r}\tilde{S}. \tag{10}$$

In the above equations the parameters with tildes represent the dimensionless counterparts. We omit the tildes from this point forward for clarity. $S=\omega/r$ is the Svanberg vorticity for numerically stable modeling of physically unstable flows [49] and Pr is the Prandtl number. A complete description of the scaling procedure can be found in Refs. [43,49].

The effective viscosity $\nu_e=\nu_0+\nu_t$. The molecular viscosity $\nu_0=\mathrm{Pr}\,\mathrm{Ra}^{-0.5}$, where the Rayleigh number $\mathrm{Ra}=\alpha g H^3 \Delta T/\nu\kappa$ and H is the height of the cavity. The eddy viscosity ν_t can be computed from the local shear rate and a length scale when the popularly used Smagorinsky model is adopted [57–59],

$$\nu_t = (C\Delta)^2|\bar{S}|, \tag{11}$$

where the constant C is called the Smagorinsky constant and is adjustable. In our simulations, we take $C=0.1$. Δ is the filter width, $\Delta=\Delta x$. Δx is the lattice grid spacing. The local intensity of the strain rate tensor is defined as

$$|\bar{S}| = \sqrt{2S_{\alpha\beta}S_{\alpha\beta}}, \tag{12}$$

where $S_{\alpha\beta}$ is the strain rate tensor and the subscripts $\{\alpha,\beta\}=\{r,z\}$.

The effective thermal diffusivity $D_e=D_0+D_t$, where $D_0=\mathrm{Ra}^{-0.5}$ and $D_t=\nu_t/\mathrm{Pr}_t$. $\mathrm{Pr}_t=0.4$ is the turbulent Prandtl number.

By the way, until now there have been many other state-of-the-art turbulence models [50–52], and they can be incorporated into the present LB model in the same way as this static Smagorinsky turbulence model.

III. LATTICE BOLTZMANN SUBGRID-SCALE MODEL FOR AXISYMMETRIC THERMAL FLOWS WITH HIGH RAYLEIGH NUMBERS

A. Coordinate transformation and axisymmetric thermal LB SGS model

By performing the following coordinate transformations [43,46,48],

$$(r,z) \mapsto (x,y), \tag{13}$$

$$(u,w) \mapsto (u,v), \tag{14}$$

Eqs. (6)–(10) can be written in the pseudo-Cartesian coordinates,

$$u = \frac{1}{x}\frac{\partial \psi}{\partial y}, \tag{15}$$

$$v = -\frac{1}{x}\frac{\partial \psi}{\partial x}, \tag{16}$$

$$\frac{\partial S}{\partial t} + u\frac{\partial S}{\partial x} + v\frac{\partial S}{\partial y} = \nu_e\left(\frac{\partial^2 S}{\partial x^2} + \frac{\partial^2 S}{\partial y^2}\right) + S_o, \tag{17}$$

$$\frac{\partial T}{\partial t} + u\frac{\partial T}{\partial x} + v\frac{\partial T}{\partial y} = D_e\left(\frac{\partial^2 T}{\partial x^2} + \frac{\partial^2 T}{\partial y^2}\right) + T_o, \tag{18}$$

$$\frac{\partial^2 \psi}{\partial y^2} + \frac{\partial^2 \psi}{\partial x^2} = \Theta. \tag{19}$$

In Eqs. (17)–(19), the source terms caused by the coordinate transformation and the buoyant forcing due to the temperature read

$$S_o = \nu_e\frac{3}{x}\frac{\partial S}{\partial x} + \mathrm{Pr}\frac{1}{x}\frac{\partial T}{\partial x}, \tag{20}$$

$$T_o = D_e\frac{1}{x}\frac{\partial T}{\partial x}, \tag{21}$$

$$\Theta = -(x^2 S + v). \tag{22}$$

Bearing in mind that here u and v stand for the velocity components along x and y coordinates.

Equations (17) (the governing equation for the flow field) and (18) (the governing equation for the temperature field), which have the same formulation except different coefficients, are nothing but advection-diffusion equations with source terms. There are many matured efficient lattice Boltzmann models for this type of equation [43]. In this paper a D2Q5 model is employed to solve these equations. It reads

$$g_k(\vec{x}+c\vec{e}_k\Delta t, t+\Delta t) - g_k(\vec{x},t) = -\tau_e^{-1}[g_k(\vec{x},t) - g_k^{(eq)}(\vec{x},t)] + \Delta t \Upsilon_{o,k}, \tag{23}$$

where $\vec{e}_k$ $(k=0,\ldots,4)$ are the discrete velocity directions,

$$\vec{e}_k = \begin{cases} (0,0), & k=0 \\ [\cos(k-1)\pi/2, \sin(k-1)\pi/2], & k=1,2,3,4, \end{cases}$$

and $c=\Delta x/\Delta t$ is the fluid particle speed. Δx, Δt, and τ_e are the lattice grid spacing, the time step, and the dimensionless effective relaxation time, respectively. $\Upsilon_{o,k}$ is the discrete form of the source term Υ_o [32,43], $\Upsilon_o = S_o, T_o$ for Eqs. (17) and (18), respectively. $\Upsilon_{o,k}$ satisfies

$$\sum_{k\geq 0} \Upsilon_{o,k} = \Upsilon_o. \tag{24}$$

The simplest choice satisfying the constraint [Eq. (24)] is

$$\Upsilon_{o,k} = \frac{\Upsilon_o}{5}. \tag{25}$$

The equilibrium distribution $g_k^{(eq)}$ is defined by

$$g_k^{(eq)} = \frac{\delta}{5}\left[1 + 2.5\frac{\vec{e}_k \cdot \vec{u}}{c}\right]. \tag{26}$$

$\delta = S, T$ for Eqs. (17) and (18), respectively, and is obtained by

$$\delta = \sum_{k\geq 0} g_k. \tag{27}$$

The method on how to evaluate τ_e for Eqs. (17) and (18) is presented in Sec. III B.

Equation (19) is just the Poisson equation, which also can be solved by the LB method efficiently. In the present study, the D2Q5 model used in our previous work [43] is employed to solve the Poisson equation. We have compared the computational efficiency of the present model with that of the traditional LB model and some conventional numerical methods. The comparison results show that the present model perhaps is the most efficient one for vortex dominated flows [30,64,65].

The evolution equation for Eq. (19) reads

$$f_k(\vec{x} + c\vec{e}_k\Delta t, t+\Delta t) - f_k(\vec{x},t) = \Omega_k + \Omega_k', \tag{28}$$

where $\Omega_k = -\tau_\psi^{-1}[f_k(\vec{x},t) - f_k^{(eq)}(\vec{x},t)]$, $\Omega_k' = \Delta t \zeta_k \Theta D$, and $D = \frac{c^2}{2}(0.5 - \tau_\psi)$. $\tau_\psi > 0.5$ is the dimensionless relaxation time [43]. $f_k^{(eq)}$ is the equilibrium distribution function and defined by

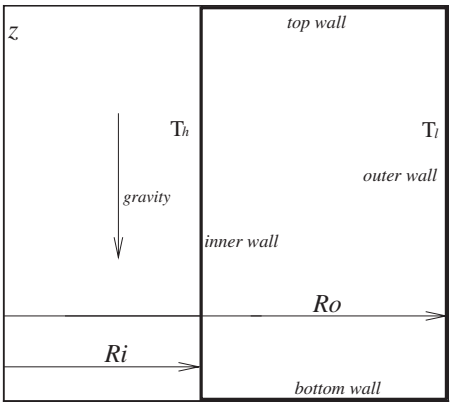

FIG. 1. The configuration of computational domain.

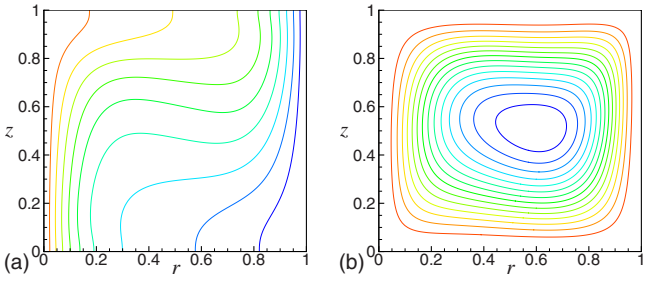

FIG. 2. (Color online) (a) Isothermal and (b) stream-function contours of natural convection at $\mathrm{Ra}=10^4$, $\mathrm{Pr}=1.0$, $A=1.0$, and $K=2.0$.

$$f_k^{(eq)} = \begin{cases} (\xi_0 - 1.0)\psi, & k=0 \\ \xi_k \psi, & k=1,2,3,4. \end{cases}$$

ξ_k and ζ_k are weight parameters given as $\xi_0 = \zeta_0 = 0$, $\xi_k = \zeta_k = 1/4$ $(k=1,\ldots,4)$. ψ is obtained by

$$\psi = \sum_{k\geq 1} f_k. \tag{29}$$

Through the Chapman-Enskog expansion, Eqs. (17)–(19) can be recovered straightforwardly from Eqs. (23) and (28), which is very similar with the process presented in Ref. [49]. To evaluate the source terms in Eqs. (17) and (18), in the present study the central difference scheme is employed. An alternative method using the moment of distribution functions to evaluate the source terms is under consideration along the line proposed in our previous work [66]. The latter seems more attractive due to its advantage of local computing.

Junk [67] has given an investigation on the relationship between the LB method and the finite difference scheme. Usual central difference scheme and the five-point stencil for the Laplacian can be obtained only for D2Q5 lattice model. More recently, van der Sman [68] carried out excellent work on the relationship between the LB method and the finite difference scheme for convection-diffusion flow. In his work, it is demonstrated that when the relaxation time equals unity, LB schemes for (convection) diffusion are equivalent to finite difference and volume schemes. However, the LB method has more degrees of freedom to make it possible to construct more accurate schemes. For some situations such

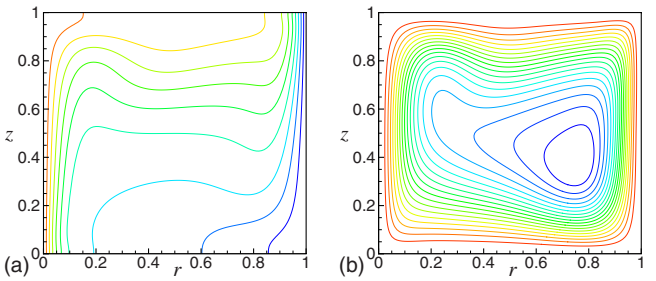

FIG. 3. (Color online) (a) Isothermal and (b) stream-function contours of natural convection at $\mathrm{Ra}=10^5$, $\mathrm{Pr}=1.0$, $A=1.0$, and $K=2.0$.

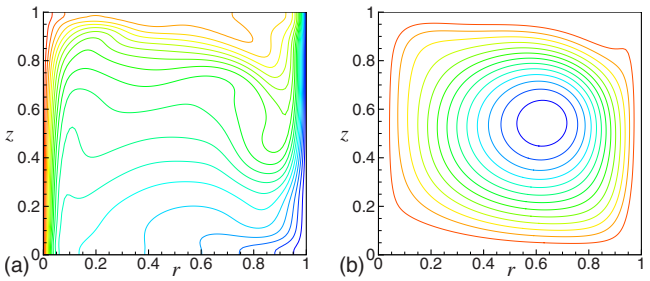

FIG. 4. (Color online) (a) Isothermal and (b) stream-function contours of natural convection at Ra=10^6, Pr=1.0, A=1.0, and K=2.0.

as grid Peclet number Pe$\gg$2, the LB method performs much better than the traditional finite difference scheme.

B. Evaluation of τ_e in the present model

The dimensionless relaxation time τ_e for Eq. (17) is determined by

$$\tau_e = \tau_0 + \frac{(C\Delta)^2|\bar{S}|}{c_s^2\Delta t}, \tag{30}$$

where $\tau_0=\frac{\nu_0}{c_s^2\Delta t}+0.5$ and $c_s^2=\frac{2}{5}c^2$.

The dimensionless relaxation time τ_e for Eq. (18) is determined by

$$\tau_e = \tau_0 + \frac{(C\Delta)^2|\bar{S}|/\mathrm{Pr}_t}{c_s^2\Delta t}, \tag{31}$$

where $\tau_0=\frac{D_0}{c_s^2\Delta t}+0.5$.

The complication of calculation of τ_e in the primitive-variable LES-based LB models results from the complication of calculation of $|\bar{S}|$ (cf. Eq. (12) in Ref. [57], Eq. (9) in Ref. [58], and Eq. (22) in Ref. [55]). Fortunately, thanks to the intrinsic features of vorticity-stream-function equations, the calculation of $|\bar{S}|$ is very simple in the present model.

For axisymmetric flow, the subscripts $\{\alpha,\beta\}=\{r,z\}$, there exists [11]

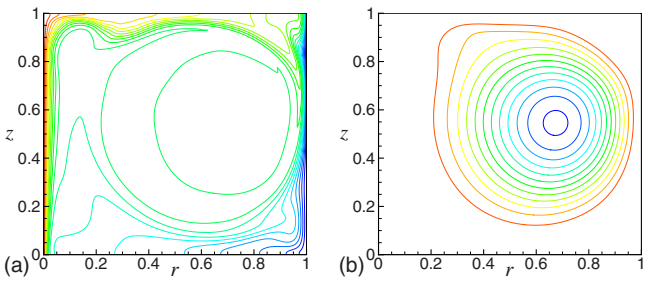

FIG. 5. (Color online) (a) Isothermal and (b) stream-function contours of natural convection at Ra=10^7, Pr=1.0, A=1.0, and K=2.0.

TABLE I. Mean Nusselt number at the inner wall with different Ra.

Ra	Present	FVM
10^4	6.2773	6.2834
10^5	11.6789	11.7710
10^6	21.6512	22.4557
10^7	35.9092	37.4398

$$2S_{\alpha\beta}S_{\alpha\beta} = 2\left[\left(\frac{\partial u}{\partial r}\right)^2 + \left(\frac{u}{r}\right)^2 + \left(\frac{\partial w}{\partial z}\right)^2\right] + \left[\frac{\partial w}{\partial r} + \frac{\partial u}{\partial z}\right]^2. \tag{32}$$

After some simple algebraic operations, Eq. (32) can become

$$2S_{\alpha\beta}S_{\alpha\beta} = 2\left[\frac{\partial u}{\partial r} + \frac{u}{r} + \frac{\partial w}{\partial z}\right]^2 + \left(\frac{\partial u}{\partial z} - \frac{\partial w}{\partial r}\right)^2 + 4\left(\frac{\partial w}{\partial r}\frac{\partial u}{\partial z} - \frac{\partial u}{\partial r}\frac{\partial w}{\partial z}\right) + 4\left(\frac{u}{r}\right)^2. \tag{33}$$

With the aid of the continuum equation [Eq. (1)] and the definition of vorticity [Eq. (5)], Eq. (33) is reduced as

$$2S_{\alpha\beta}S_{\alpha\beta} = \omega^2 + 4\left(\frac{\partial w}{\partial r}\frac{\partial u}{\partial z} - \frac{\partial u}{\partial r}\frac{\partial w}{\partial z}\right) + 4\left(\frac{u}{r}\right)^2. \tag{34}$$

For incompressible low Mach flow, there exists [69]

$$\nabla^2 p = 2\left(\frac{\partial w}{\partial r}\frac{\partial u}{\partial z} - \frac{\partial u}{\partial r}\frac{\partial w}{\partial z}\right) + \mathcal{O}(\mathrm{Ma}^2) \tag{35}$$

(where Ma is the Mach number). Therefore Eq. (34) becomes

$$2S_{\alpha\beta}S_{\alpha\beta} = \omega^2 + 2\nabla^2 p + 4\left(\frac{u}{r}\right)^2 + \mathcal{O}(\mathrm{Ma}^2). \tag{36}$$

For low Mach flow, there also exist $\mathcal{O}(\nabla p)\sim\mathcal{O}(\mathrm{Ma}^2)$ and $\mathcal{O}(u)\sim\mathcal{O}(\mathrm{Ma})$ [28,69]. Therefore Eq. (36) is further reduced as

$$2S_{\alpha\beta}S_{\alpha\beta} = \omega^2 + \mathcal{O}(\mathrm{Ma}^2). \tag{37}$$

Consequently,

$$|\bar{S}| = \sqrt{2S_{\alpha\beta}S_{\alpha\beta}} = |\omega| = |rS|, \tag{38}$$

with second-order accuracy of $\mathcal{O}$(Ma) consistent with the numerical accuracy of the LB method [28].

TABLE II. Mean Nusselt number at the inner wall with different Pr.

Pr	Present	Ref. [10]
0.73	6.1198	6.13
1.0	6.2773	6.17
7.0	6.5334	6.36
25.0	6.2299	6.31

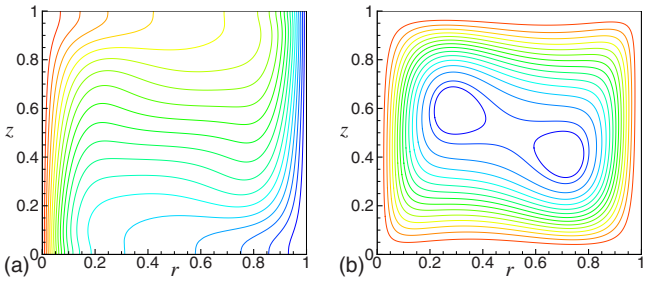

FIG. 6. (Color online) (a) Isothermal and (b) stream-function contours of natural convection at Ra=10^5, Pr=0.7, A=1.0, and K=1.0.

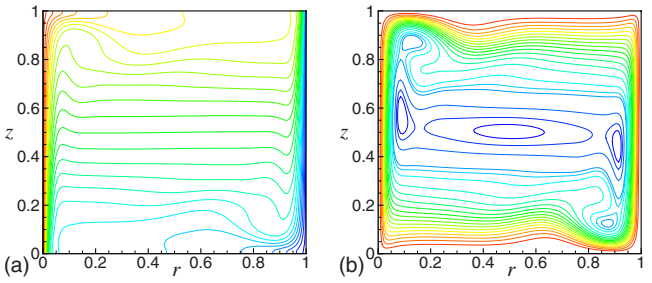

FIG. 8. (Color online) (a) Isothermal and (b) stream-function contours of natural convection at Ra=10^7, Pr=0.7, A=1.0, and K=1.0.

Because the value of Svanberg vorticity S is already known at each grid point, therefore compared with primitive-variable LES-based LB models [55,57,58] no extra computational cost needed for $|\bar{S}|$ in the present model.

IV. NUMERICAL RESULTS

In the present study, natural convection in an enclosed circular annular cavity formed by two concentric vertical cylinders is simulated to validate the present model. The configuration of the vertical annulus is illustrated in Fig. 1. The inner wall has the radius R_i and the outer wall has R_o. $K=R_o/R_i$ is the radius ratio. The aspect ration $A=H/(R_o-R_i)$. H is the height of the annular cavity.

The boundary conditions are the following: $\psi=u=w=0$ at all walls; $T_h=1.0$ at the inner wall; $T_l=-1.0$ at the outer wall; and $\partial T/\partial z=0$ at the top and bottom walls. The initial conditions are $\psi=u=w=0$ and $T=0$. The value of Svanberg vorticity S at walls is calculated using the method proposed in Ref. [43].

A. Radius ratio $K \neq 1.0$

The first case is $K=2.0$ and $A=1.0$, which is a benchmark test popularly used in previous work [9,10]. Figures 2–5 illustrate the isothermal and stream-function contours for Ra varying from 10^4 to 10^7 and Pr=1.0. The grid resolution is 100×100. When Ra$<10^6$, the flows are steady. There is a large clockwise thermal recirculation with the isotherms not being horizontally uniform in the core region within the enclosure. The stratification of the isotherms is mostly confined to the zones adjacent to the sidewalls. While Ra$\geq10^6$, the flows become unsteady. There also exists a large clockwise thermal recirculation, but the vortex center will move along with time. The isotherms are distorted and more significantly for higher Ra. The zones of the stratification of the isotherms become narrower with Ra increasing. The shape of the isotherms shows how the dominant heat transfer mechanism changes as Ra increases. For low Ra almost vertical isotherms appear because heat is transferred by conduction between hot and cold walls. As the isotherms depart from the vertical position, the heat transfer mechanism changes from conduction to convection. The contour plots obtained by the present model agree well with that in previous work [9,10].

To quantify the results, the mean Nusselt number Nu at the inner wall [10] obtained by the present model are listed in Table I, with that obtained by the finite volume method (FVM) solver (FLUENT). The results obtained by the present model agree well with that obtained by the FVM.

From the data in Table I we can get

$$\mathrm{Nu} \approx 0.744\,35 \times \mathrm{Ra}^{0.241\,01}, \tag{39}$$

which agrees with the exponent relationship concluded in Refs. [9,10].

In addition, Table II lists the Nu with different Pr while Ra=10^4. The numerical data published in Ref. [10] are also listed in the table for comparison. One can see that the present model works well for a large range of Pr.

B. Radius ratio $K=1.0$

The second case is $K=1.0$ and $A=1.0$, which is reduced to a square cavity formed by two plane walls [5–8], as men-

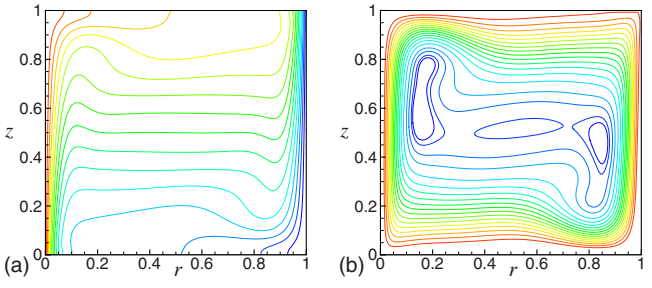

FIG. 7. (Color online) (a) Isothermal and (b) stream-function contours of natural convection at Ra=10^6, Pr=0.7, A=1.0, and K=1.0.

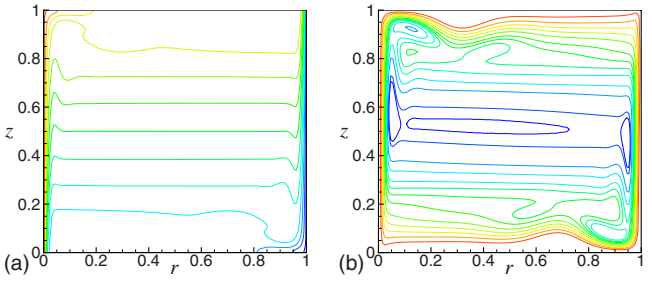

FIG. 9. (Color online) (a) Isothermal and (b) stream-function contours of natural convection at Ra=10^8, Pr=0.7, A=1.0, and K=1.0.

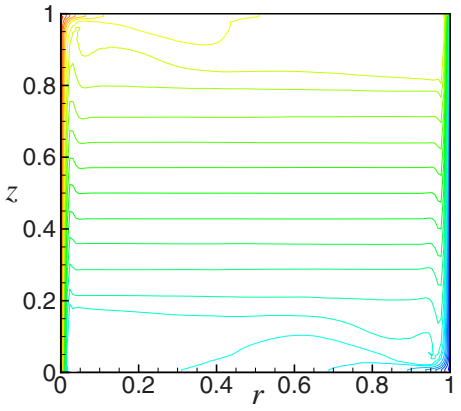

FIG. 10. (Color online) Isothermal contours of natural convection at Ra=10^9, Pr=0.7, A=1.0, and K=1.0.

tioned in Sec. I. In our simulation, that K=1.0 is implemented by setting R_i=$10^4(R_o-R_i)$. And Pr=0.7 in the following simulations. The grid resolution 350×350 is used to guarantee the numerical stability for turbulence simulation.

Figures 6 and 7 show the isothermal and stream-function contours at Ra$\leq10^6$. There are two vortex centers at Ra =10^5. When Ra continues increasing, the two vortices move toward the walls, giving space for a third vortex to develop. Even for higher Ra=10^6, the third vortex is very weak in comparison with the other two.

As $10^7\leq$Ra$\leq10^8$, the transitional flows appear. The velocities at the center of the cavity are very small compared with those at the boundaries where the fluid is moving fast, forming vortices at the lower right and top left corner of the cavity, destabilizing the laminar flow, as Figs. 8 and 9 illustrate. The vortices become narrow when Ra increases, improving the stratification of the flow at the central part of the cavity. The isotherms at the center of the cavity are horizontal and become vertical near the walls. The transitional flow features reported by previous studies [5–8] are well captured by our model.

When Ra$\geq10^9$, the flow becomes fully turbulent. The flow structure in entire simulation domain becomes irregular and chaotic. The isothermal curves become almost straight at the center and very sharp inside the very thin boundary layers, as Fig. 10 shows.

Table III reports the Nu, together with that published in previous studies [5,70]. From this table one can see that the grid resolution is enough near the wall. The deviations of Nu between different models perhaps result from the effect of the eddy viscosity ν_t becoming significant when Ra$\geq10^9$. Because LES is inherently dependent on the grid resolution, therefore no final grid-independent result exists [71].

TABLE III. Comparison of mean Nusselt number at the inner wall of convectional flow with previous works.

Ra	Ref. [5]	Ref. [70]	Present
10^5	4.5226	4.518	4.5634
10^6	8.805	8.792	8.8547
10^7	16.79	16.408	16.6794
10^8	30.506	29.819	30.5334
10^9	57.350		50.3504

V. CONCLUSION

In order to simulate convectional flow with high Ra within an enclosed circular annular cavity formed by two concentric vertical cylinders, in the present study a simple LB SGS model for such flow is designed. The evaluation of τ_e in the present model is quite easy and efficient. The numerical experiments demonstrate that the present model works well for a large range of Ra and Pr. Though in the present study a popularly used static Smagorinsky turbulence model is adopted to demonstrate how to develop a LB SGS model for simulating axisymmetric thermal flows with high Rayleigh numbers, other state-of-the-art turbulence models can be incorporated into the present model in the same way. In addition, the present model can be extended straightforwardly to simulate other axisymmetric convectional flows with high Ra, for example, turbulent convection with internal volumetric heat generation in a vertical cylinder [12,13].

ACKNOWLEDGMENTS

This work was partially supported by the Alexander von Humboldt Foundation, Germany. The present authors would gratefully acknowledge the referees for their helpful advice and comments.

[1] K. Stork and U. Muller, J. Fluid Mech. **71**, 231 (1975).
[2] M. Cawley and P. McBride, Int. J. Heat Mass Transfer **47**, 1175 (2004).
[3] J. A. Deiber and R. A. Bortolozzi, Chem. Eng. Sci. **53**, 1505 (1998).
[4] M. El-Shaarawi and A. Negm, Heat Mass Transfer **35**, 133 (1999).
[5] H. N. Dixit and V. Babu, Int. J. Heat Mass Transfer **49**, 727 (2006).
[6] N. C. Markatos and K. A. Pericleous, Int. J. Heat Mass Transfer **27**, 755 (1984).
[7] G. De Vahl Davis, Int. J. Numer. Methods Fluids **3**, 249 (1983).
[8] P. Le Quéré, Comput. Fluids **20**, 29 (1991).
[9] G. de Vahl Davis and R. W. Thomas, Phys. Fluids **12**, II-198 (1969).
[10] T. Schwab and K. Witt, AIChE J. **16**, 1005 (1970).
[11] E. Papanicolaou and V. Belessiotis, Int. J. Heat Mass Transfer **45**, 1425 (2002).
[12] A. Sharma, K. Velusamy, and C. Balaji, Ann. Nucl. Energy **35**, 1502 (2008).
[13] M. Holzbecher and A. Steiff, Int. J. Heat Mass Transfer **38**,

2893 (1995).
[14] J. Sorensen, S. Kristensen, and L. Christensen, Lect. Notes Comput. Sci. **1184**, 631 (1996).
[15] C. Yung, T. Keith, Jr., and K. Witt, Int. J. Numer. Methods Fluids **9**, 167 (1989).
[16] D. Xu, B. Khoo, and M. Leschziner, Int. J. Numer. Methods Heat Fluid Flow **8**, 245 (1998).
[17] H. Laux, S. Johansen, H. Berg, and O. Klevan, Scand. J. Metall. **29**, 71 (2000).
[18] H. Berg, H. Laux, S. T. Johansen, and O. S. Klevan, Ironmaking Steelmaking **26**, 127 (1999).
[19] H. Hajikandi and A. Mansoori, J. Appl. Sci. **7**, 121 (2007).
[20] R. J. Poole and M. P. Escudier, J. Non-Newtonian Fluid Mech. **117**, 25 (2004).
[21] H. Yapici, N. Kayatas, N. Kahraman, and G. Bastürk, Entropy **7**, 38 (2005).
[22] H. Yapici, G. Baştürk, N. Kayataş, and S. Yalçin, Sadhana: Proc., Indian Acad. Sci. **30**, 625 (2005).
[23] A. Randriamampianina, R. Schiestel, and M. Wilson, Int. J. Heat Fluid Flow **25**, 897 (2004).
[24] R. Jacques, P. Le Quéré, and O. Daube, Int. J. Heat Fluid Flow **23**, 381 (2002).
[25] K. Mohseni, Phys. Fluids **13**, 1924 (2001).
[26] Y. Qian, D. d'Humieres, and P. Lallemand, Europhys. Lett. **17**, 479 (1992).
[27] R. Benzi, S. Succi, and M. Vergassola, Phys. Rep. **222**, 145 (1992).
[28] S. Chen and G. D. Doolen, Annu. Rev. Fluid Mech. **30**, 329 (1998).
[29] S. Succi, *The Lattice Boltzmann Equation for Fluid Dynamics and Beyond* (Oxford University Press, Oxford, 2001).
[30] S. Chen, J. Tölke, and M. Krafczyk, Comput. Methods Appl. Mech. Eng. **198**, 367 (2008).
[31] S. Succi, E. Foti, and F. Higuera, Europhys. Lett. **10**, 433 (1989).
[32] S. P. Dawson *et al.*, Comput. Chem. Eng. **19**, 617 (1995).
[33] H. Chen *et al.*, Science **301**, 633 (2003).
[34] S. Chen *et al.*, Appl. Math. Comput. **193**, 266 (2007).
[35] G. Hazi *et al.*, Ann. Nucl. Energy **29**, 1421 (2002).
[36] D. Yu *et al.*, Prog. Aerosp. Sci. **39**, 329 (2003).
[37] S. Chen, Z. Liu, B. Shi, Z. He, and C. Zheng, Acta Mech. Sin. **21**, 574 (2005).
[38] I. Ginzburg, Adv. Water Resour. **28**, 1171 (2005).
[39] S. Chen *et al.*, Int. J. Mod. Phys. C **18**, 187 (2007).
[40] S. Arcidiacono, J. Mantzaras, and I. V. Karlin, Phys. Rev. E **78**, 046711 (2008).
[41] D. Raabe, Modell. Simul. Mater. Sci. Eng. **12**, R13 (2004).
[42] J. Meng, Y. Qian, X. Li, and S. Dai, Phys. Rev. E **77**, 036108 (2008).
[43] S. Chen, J. Tölke, S. Geller, and M. Krafczyk, Phys. Rev. E **78**, 046703 (2008).
[44] J. G. Zhou, Phys. Rev. E **78**, 036701 (2008).
[45] T. Reis and T. N. Phillips, Phys. Rev. E **75**, 056703 (2007).
[46] Y. Peng, C. Shu, Y. T. Chew, and J. Qiu, J. Comput. Phys. **186**, 295 (2003).
[47] I. Halliday, L. A. Hammond, C. M. Care, K. Good, and A. Stevens, Phys. Rev. E **64**, 011208 (2001).
[48] H. Huang, T. S. Lee, and C. Shu, Int. J. Numer. Methods Fluids **53**, 1707 (2007).
[49] S. Chen, J. Tölke, and M. Krafczyk, Phys. Rev. E **79**, 016704 (2009).
[50] J. K. Wang and R. E. Milane, Int. J. Numer. Methods Fluids **50**, 27 (2006).
[51] M. Lesieur and O. Metais, Annu. Rev. Fluid Mech. **28**, 45 (1996).
[52] H. Pitsch, Annu. Rev. Fluid Mech. **38**, 453 (2006).
[53] S. Hou, J. Sterling, S. Chen, and G. D. Doolen, Fields Inst. Commun. **6**, 151 (1996).
[54] C. Teixeira, Int. J. Mod. Phys. C **9**, 1159 (1998).
[55] M. Krafczyk, J. Tölke, and L. Luo, Int. J. Mod. Phys. B **17**, 33 (2003).
[56] H. Yu, L. Luo, and S. Girimaji, Comput. Fluids **35**, 957 (2006).
[57] H. J. Liu *et al.*, Int. J. Heat Mass Transfer **49**, 4672 (2006).
[58] Y. Dong and P. Sagaut, Phys. Fluids **20**, 035105/1 (2008).
[59] M. J. Pattison, K. N. Premnath, and S. Banerjee, Phys. Rev. E **79**, 026704 (2009).
[60] S. Chen and M. Krafczyk, Int. J. Therm. Sci. (to be published).
[61] J. Ravnik, L. Skerget, and M. Hribersek, Eng. Anal. Boundary Elem. **30**, 671 (2006).
[62] R. Milane, Int. J. Numer. Methods Fluids **44**, 837 (2004).
[63] P. Wang and X. Bai, Int. J. Numer. Methods Fluids **47**, 99 (2005).
[64] S. Chen, J. Tölke, and M. Krafczyk, Phys. Rev. E **80**, 016702 (2009).
[65] S. Chen, Appl. Math. Comput. (to be published).
[66] J. Tölke, J. Comput. Theor. Nanosci. **3**, 579 (2006).
[67] M. Junk, Numer. Methods Partial Differ. Equ. **17**, 383 (2001).
[68] R. G. M. van der Sman, Comput. Fluids **35**, 849 (2006).
[69] T. J. Chung, *Computational Fluid Dynamics* (Cambridge University Press, Cambridge, 2002).
[70] F. Kuznik, J. Vareilles, G. Rusaouen, and G. Krauss, Int. J. Heat Fluid Flow **28**, 862 (2007).
[71] D. Barhaghi, L. Davidson, and R. Karlsson, Int. J. Heat Fluid Flow **27**, 811 (2006).